CHEMISTRY OF MATERIALS

pubs.acs.org/cm

Article

Solution Processable Pseudo *n*-Thienoacenes via Intramolecular S···S Lock for High Performance Organic Field Effect Transistors

Sureshraju Vegiraju,[#] Xian-Lun Luo,[#] Long-Huan Li, Shakil N. Afraj, Chi Lee, Ding Zheng, Hsin-Chun Hsieh, Chia-Chi Lin, Shao-Huan Hong, Hsin-Chia Tsai, Gene-Hsiang Lee, Shih-Huang Tung, Cheng-Liang Liu,* Ming-Chou Chen,* and Antonio Facchetti*

Cite This: *Chem. Mater.* 2020, 32, 1422−1429

Read Online

ACCESS | Metrics & More | Article Recommendations | Supporting Information

ABSTRACT: New solution processable 3,5-dithioalkyl dithienothiophene (DSDTT) based small molecular semiconductors end functionalized with various (fused) thiophenes including dithienothiophene (DTT), thienothiophene (TT), and thiophene (T) are synthesized and characterized in organic field effect transistors (OFETs). The new DSDTT core was synthesized via a one-pot [1 + 1 + 1] methodology. For comparison, non-thiolated 3,5-dialkyl dithienothiophene (DRDTT) based molecules are also prepared and characterized. Optical, electrochemical, and computed electronic structures of these molecules are investigated and contrasted. Single crystal data support evidence of S(alkyl)··· S(thiophene) intramolecular locks, with a very short intramolecular S−S distance of 3.17 Å, planarizing the structure as for the equivalent extended *n*-thienoacenes. Via a solution-shearing semiconductor film deposition method, these semiconductors exhibit a OFET hole mobility up to 2.6 $cm^2\ V^{-1}\ s^{-1}$, the greatest reported to date for fused/all-thiophene based small molecular organic semiconductors.

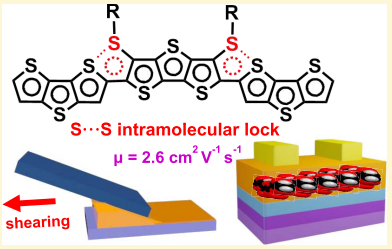

INTRODUCTION

Organic semiconductor materials have been investigated for possible application in organic optoelectronic devices due to their unique features enabling mechanical flexibility, light weight, and low cost compared to traditional silicon based technologies.[1−3] Therefore, the development of novel π-conjugated small molecule and polymeric materials have received much attention from both academia and industry.[4−14] Small molecules have the advantages of a well-defined molecular weight, facile purification and good batch-to-batch reproducibility compared to many polymers.[15−18] Several factors need to be considered when designing novel solution processable small molecules to achieve good charge transport characteristics. For example, an organic semiconductor must contain a planar π-conjugated backbone to promote π−π stacking through intermolecular orbital overlap, have solubilizing groups for easy processability and exhibit good environmental stability.[19−21] Thus, numerous strategies have been employed for developing novel π-conjugated cores.[22−24] Among them, fused thiophenes and their derivatives have been widely explored and it was shown that they exhibit highly planar structures, strong intermolecular S···S interactions and extensive conjugation, therefore, they become one of the important building blocks for organic electronics.[25−27] Despite of these advantages fused thiophenes with more than five fused rings are difficult to synthesize, exhibits low solubility, and very poor charge transport characteristics. For example, the reported organic field effect transistors (OFETs) mobilities of pentathienoacene (PTA)[28,29] and hexathienoacene (HTA)[30] (Figure 1a) are only up to 0.045 and 0.06 $cm^2\ V^{-1}\ s^{-1}$. A strategy to achieve considerable molecular planarization yet enhanced solubility consists of employing intramolecular S···X interactions (X = O, N, S, halogens, see examples in Figures 1b and S1), this strategy is also able to increase molecular orbital delocalization and improve device performances.[24,31−37] For instance, for oligothiophenes having heteroalkyl substituents in the β position possess attractive interactions between the heteroatom and the sulfur locks and the structure dramatically reducing the torsional angle between aromatic rings versus conventional alkyl substituents.[32,38]

Recently we have reported this strategy for dithioalkylbithiophene (SBT) based organic semiconductors (Figure 1c), in which we demonstrated that the four sulfur atoms in the two thioalkyl chains and the bithiophene in SBT unit are completely planar and locked at a S(alkyl)···S(thiophene) intramolecular distance of ∼3.09 Å, substantially lower that of the van der Waals radius sum of two S atoms (∼3.6 Å). A field-effect hole mobility of 1.7 $cm^2\ V^{-1}\ s^{-1}$ was achieved in OFETs for a solution-sheared film.[39] Inspired by these results, combining two dithienothiophenes[40−45] with planar SBT to improve the device performances of fused thiophenes, and considering the very limited number of structures explored

Received: September 26, 2019
Revised: January 14, 2020
Published: February 10, 2020

Downloaded via NATL TAIWAN UNIV on February 26, 2020 at 07:30:19 (UTC).
See https://pubs.acs.org/sharingguidelines for options on how to legitimately share published articles.

© 2020 American Chemical Society

https://dx.doi.org/10.1021/acs.chemmater.9b03967
Chem. Mater. 2020, 32, 1422−1429

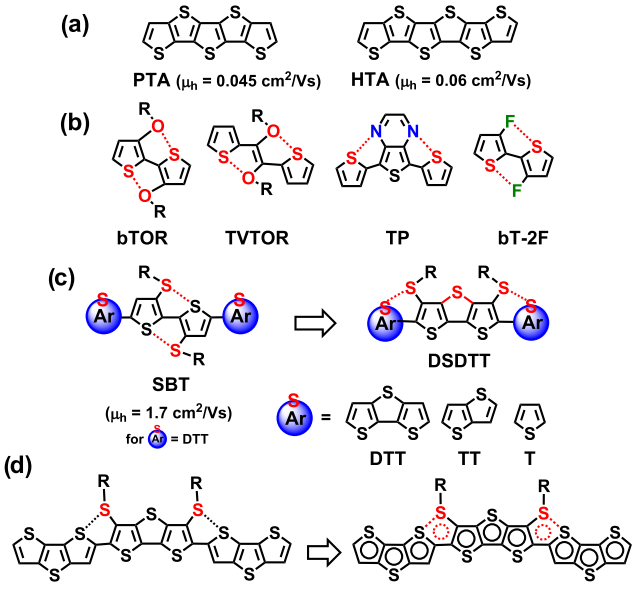

Figure 1. Chemical structures of (a) fused-thiophene semiconductors of PTA and HTA. (b) Polymeric building blocks containing S···X conformational locks. (c) dithioalkylbithiophene (SBT) and 3,5-dithioalkyl dithienothiophene (DSDTT) semiconductors examined in this study. (μ_h is hole mobilities in $cm^2\ V^{-1}s^{-1}$.) (d) Schematic representation of compound 1, which acting like a highly soluble and solution processable undeca-thienoacene.

using intramolecular locks using S···S interactions, here we report a new dithioalkyl substituted dithienothiophene (DSDTT) core end-capped with different heteroarenes including DTT, thienothiophene (TT), and thiophene (T) (Figure 1c). Note, the new DSDTT core can be obtained in a one-pot synthetic strategy.[46] For comparison, the corresponding non-thioakyl dithienothiophene (DRDTT) based molecules were also synthesized (see Scheme 1). Our data suggest that this new DSDTT-heteroarene molecular design, enabling pseudo-fused *n*-thienoacene structures (Figure 1d), affords highly soluble, yet considerably planarized, small molecular semiconductors for optoelectronics. Charge transport measurements demonstrate a hole mobility up to 2.6 $cm^2\ V^{-1}\ s^{-1}$, which is the highest mobility value within the fused-thiophene OTFT family, with the previous record of 1.8 $cm^2\ V^{-1}\ s^{-1}$ obtained for single-crystal based devices.[47] Thus, this study can further promote the use of fused thiophenes and S···S interactions for new optimal organic semiconductors.

Scheme 1. Synthetic Route to the Final Compounds

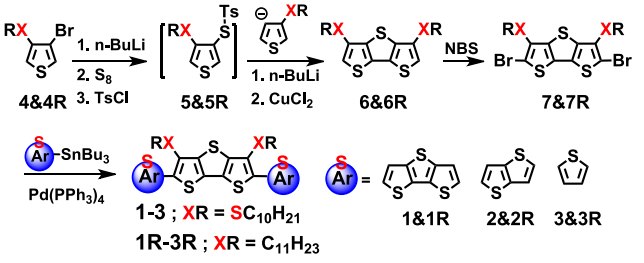

RESULTS AND DISCUSSION

In this section we first report the synthesis of the new molecular semiconductors followed by evaluation of their physical properties using several characterization techniques. Next, we compare and contrast the molecular structure and packing characteristics of thioalkyl- vs alkyl-functionalized DSDTTs using single crystal data. We then fabricate thin-films of all semiconductors using a shear method and evaluated the charge transport properties by fabricating thin-film transistors. Finally, we characterize the semiconductor film morphology and microstructure to rationalize, in combination with the physical and crystal data, trends in charge transport.

Synthesis. The synthetic route to all the new structures is presented in Scheme 1 where the new central DSDTT (6) core was prepared the first time via a one-pot reaction and DRDTT (6R) was synthesized according to literature procedures.[45] For the one-pot reaction to prepare the DSDTT core, 3-bromo-4-thioalkylthiophene (4) was lithiated using *n*-BuLi, next S_8 and then TsCl were added to form the intermediate 5. The mixture was treated with 3-lithium-4-thioalkyl thiophene, followed by a dilithiation with *n*-BuLi, and then ring closure by $CuCl_2$, to give the dithioalkylated DSDTT (6) in ∼30% yield. The DSDTT core was then brominated and next end-capped with various stannylated conjugated aryl (Ar) units, such as DTT, TT, and T to produce the small molecules 1−3, respectively. For comparison, the dialkyl DRDTTs (1R−3R) were also synthesized [for details see the Supporting Information (SI)].

Physical Characterization. The thermal properties of six new small molecules were evaluated by differential scanning calorimetry (DSC, Figure S2) and thermogravimetric analysis (TGA, Figure S3). DSC data show that DSDTT compounds have slightly higher melting points (173−63 °C) compared to the alkylated compounds (165−91 °C) except 3 and 3R. TGA analysis reveals that all compounds have good thermal stability, with ∼5 wt % loss occurring at >327 °C. The solution optical absorption spectra of all compounds in dilute 1,2-dichlor-

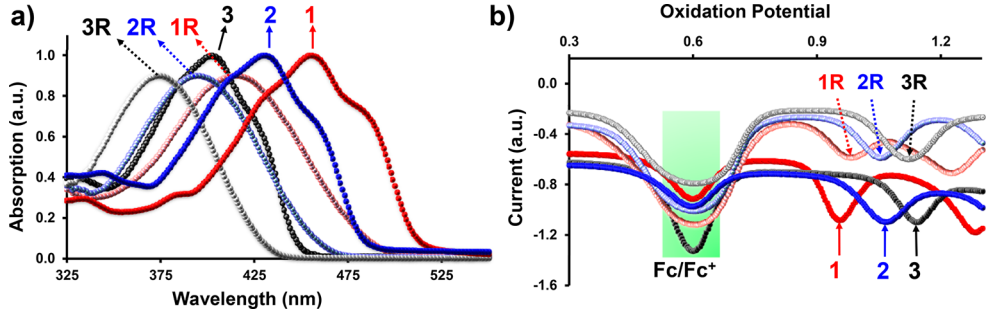

Figure 2. (a) Optical spectra of DSDTTs (1−3) and DRDTTs (1R−3R) in *o*-dichlorobenzene solution. (b) Oxidation potential curves of all compounds in *o*-dichlorobenzene. Fc^+/Fc was used as the internal standard (at +0.6 V) for the determination of the electrochemical potentials. Oxidation potential curves >1.30 V were omitted and baselines of 1R−3R are adjusted for clarity.

https://dx.doi.org/10.1021/acs.chemmater.9b03967
Chem. Mater. 2020, 32, 1422−1429

Table 1. Thermal, Electrochemical, Optical Properties, and OFET Performances of the Indicated Compounds

compound	T_m[a] (°C)	T_d[b] (°C)	λ_{max}[c] (nm)	E_{ox}[d] (V)	E_{red} (V)	HOMO (eV)	LUMO (eV)	E_g (eV)	μ_{max} (μ_{avg})[h] ($cm^2 V^{-1} s^{-1}$)	I_{ON}/I_{OFF}	V_{th}[h] (V)
1	173	350	454	0.95	−1.66	−5.15	−2.54	2.38	2.6 (1.6 ± 0.5) × 10^0	10^4–10^5	−25.7 ± 15.8
2	136	344	431	1.06	−1.80	−5.27	−2.40	2.51	9.6 (5.3 ± 2.4) × 10^{-2}	10^4–10^5	−12.3 ± 3.9
3	63	327	402	1.14	−2.00	−5.34	−2.20	2.75	2.3 (1.4 ± 0.8) × 10^{-5}	10^2–10^3	9.2 ± 12.7
1R	165	366	416	0.98	n.d[e]	−5.18	−2.68[f]	2.50[g]	3.9 (2.6 ± 0.9) × 10^{-2}	10^5–10^6	−21.6 ± 4.8
2R	106	374	395	1.06	n.d[e]	−5.27	−2.60[f]	2.67[g]	1.8 (1.2 ± 0.6) × 10^{-3}	10^5–10^6	−29.2 ± 9.0
3R	91	332	374	1.12	n.d[e]	−5.36	−2.5[f]	2.85[g]	n.d[e]	n.d[e]	n.d[e]

[a]By DSC. [b]By TGA. [c]In *o*-$C_6H_4Cl_2$. [d]By DPV in *o*-DCB, E_{ox} = oxidation potential, E_{red} = reduction potential. HOMO = −(4.2 + E_{ox}); LUMO = −(4.2 + E_{red}). [e]Not determined. [f]HOMO + E_g. [g]From onset of the optical absorption. [h]Average of at least 10 devices.

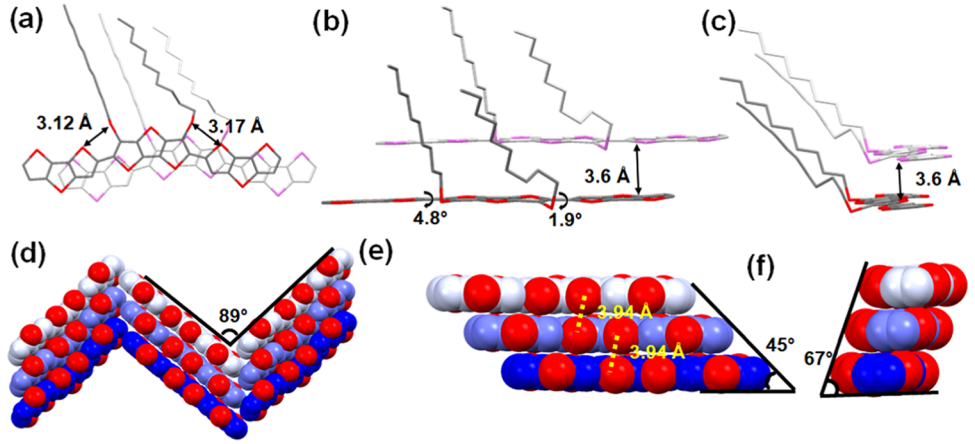

Figure 3. Single crystal structure of 1 in stick (a–c) and space filling models (d–f). (a) Top view of two stacking DSDTT molecules. The S(Thio)···S(R) intramolecular distances are ∼3.12 and 3.17 Å. (b) Front view. (c) Side view of two stacking DSDTT molecules. The interplanar distance between the DSDTT layers. (d) Herringbone packing of DSDTT molecules in a space filling model. The alkyl chains are omitted for clarity. (e, f) The slipping angles of the DSDTT stacks.

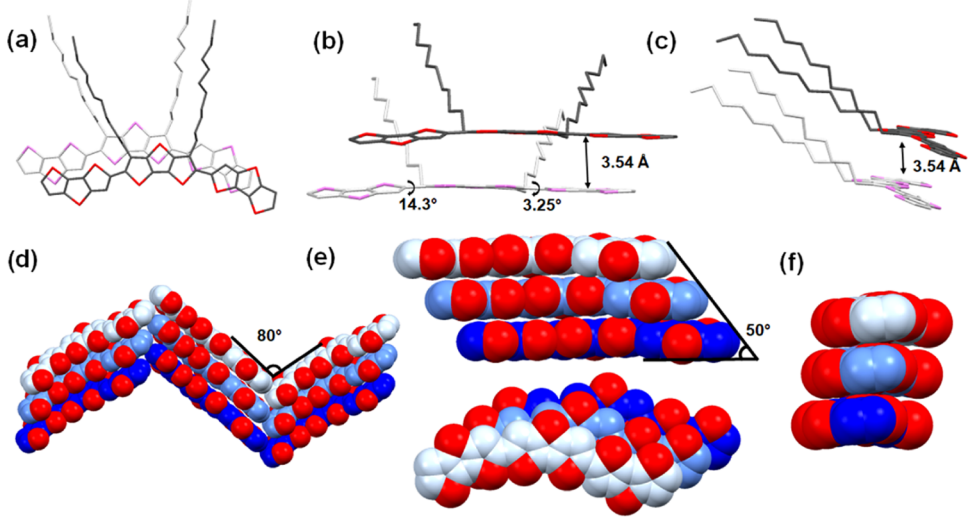

Figure 4. Single crystal structure of 1R. (a) Top view of two stacking DRDTT molecules. (b) Front view of two stacking DRDTT molecules. (c) Side view of two stacking DRDTT molecules. The interplanar distance between the DRDTT layers. (d) Herringbone packing of DRDTT molecules in space filling model. (e, f) Front, top, and side views of DRDTTs in space filling model.

obenzene (DCB) solutions are shown in Figure 2a, and the data is summarized in Table 1. With increasing the end-capped aromatic extension connected to the central DSDTT or DRDTT cores, the absorption maxima [λ_{max}, 402 → 454 nm for 3 → 1; 374 → 416 nm for 3R → 1R] and onsets [λ_{onset}, 440 → 525 nm for 3 → 1; 475 → 500 nm for 3R → 1R] are significantly red-shifted. Furthermore, the abovementioned absorption values for the thioalkylated DSDTTs (1–3) are significantly red shifted by ∼30 nm compared to the non-thioalkylated DRDTTs (1R–3R), indicating enhanced π-conjugation for the DSDTT structures by intramolecular S···S lock (vide infra). To understand whether the intramolecular S···S lock contribute to compound 1 planarization or not, solution temperature-dependent UV–vis measurements were carried out for compounds 1 and 1R. Clearly Figure S4 shows that as the temperature increases from 25 to 85 °C (ΔT = 60

https://dx.doi.org/10.1021/acs.chemmater.9b03967
Chem. Mater. 2020, 32, 1422–1429

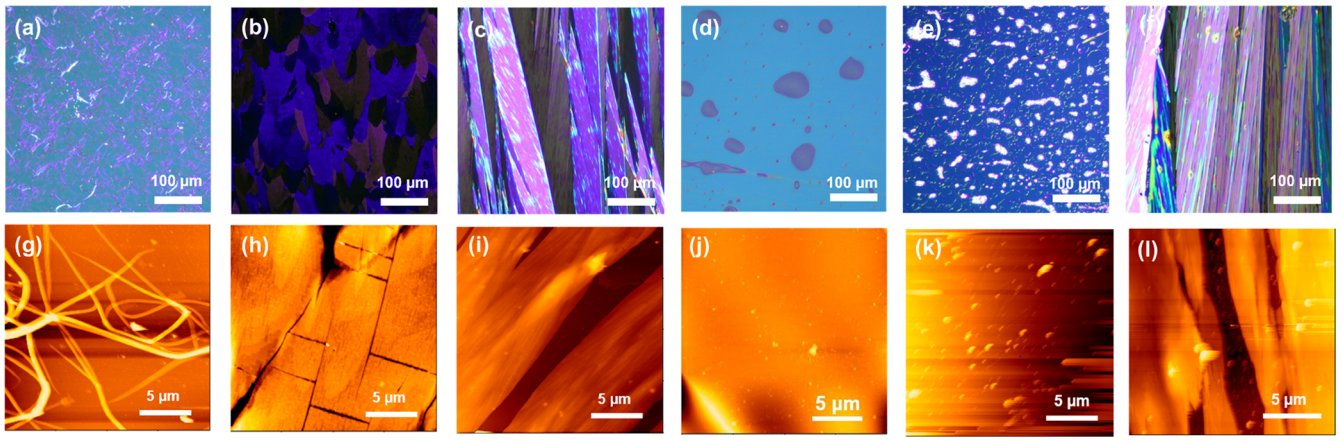

Figure 5. POM and atomic force microscopy (AFM) images, respectively, of 3 (a, g), 2 (b, h), 1 (c, i), 3R (d, j), 2R (e, k) and 1R (f, l) thin film.

°C), the optical absorption profile and λ_{max} of 1R do not change. In contrast, the λ_{max} of compound 1 substantially blue shifted by ∼12 nm. This data indicates that the electronic structure in solution of compound 1 is strongly affected at higher temperatures, with a reduction of effective π-conjugation. Thus, intramolecular S···S interactions planarizing the DSDTT unit, as further demonstrated by the crystal structure analyses (vide infra), become less effective of enhanced inter-ring motions.[27] In solution-sheared films, processed similar to those used in OFET measurements (vide infra), the absorbance spectra of all molecules are broader and red shifted compared to the solution ones (Figure S5). The vibronic shoulder appearing at longer wavelengths (∼530 nm for 1) indicates the existence of ordered aggregates and effective backbone π-stacking in the solid state. The electrochemical properties (Table 1) were investigated using differential pulse voltammetry (DPV) in *o*-$C_6H_4Cl_2$ [ortho-dichlorobenzene (*o*-DCB), 0.1 M Bu_4NPF_6, 25 °C]. Representative oxidation potential plots are displayed in Figure 2b. The oxidation peaks (E_{ox}) of DSDTTs [+0.95 (1), +1.06 (2), +1.14 V (3)] are close to those of DRDTTs [+0.98 (1R), +1.06 (2R), and +1.12 V (3R)]. The calculated highest occupied molecular orbital (HOMO) and lowest unoccupied molecular orbital (LUMO) energy levels of 1−3 and 1R−3R are reported in Table 1 (see footnote for calculation details). As expected, going from the T to the DTT end-functionalization, the HOMO/LUMO values of 3 → 1 and 3R → 1R are up-/down-shifted by 0.19/∼0.54 and 0.18/∼0.17 eV, respectively, due to the energy gap contracting. All the above data are consistent with density functional theory (DFT)-derived molecular orbital computations, as shown in Figure S6 of the SI.

Single Crystal Structure. Single crystals of molecules 1 and 1R were achieved by slow solvent evaporation and are shown in Figures 3, 4, S7, and S8, and the data is summarized in Tables S1 and S2. Molecule 1 crystallizes in a monoclinic $P2_1/c$ space group with both thioalkyl chains lying on the same side of the conjugated DSDTT backbone. The intramolecular distances of two S(DTT)···S(R) are ∼3.12 and 3.17 Å (Figure 3a). These distances are well below the sum of the van der Waals radii of two S atoms (∼3.6 Å), which suggests that the two sulfur atoms are locked through intramolecular interactions. The end-capping DTT units are almost coplanar to the central DSDTT core and the core-DDT dihedral angles are only 4.8 and 1.9°. In contrast for alkylated 1R, the alkyl side chains forces the end-capped DTT units to rotate by 14.3 and 3.2° with respect the DRDTT core (Figure S8), and the two DTT units are asymmetrically oriented along the DRDTT core. Both the molecules stack in a two face-to-face columnar fashion and crystalize in a herringbone-packing motif (Figures S7 and S8). For 1, the shortest face-to-face intermolecular planar distance of two DSDTT molecules is 3.60 Å (Figure 3b,c), with a herringbone angle of 89° as well as slipping angles of 45 and 67° (Figure 3d−f). Among the two columnar stacks, the shortest intermolecular S···S distances are 3.36−3.44 Å for 1 (Figure S7) and 3.48−3.83 Å for 1R (Figure S8). These short packing distances of intra- and intermolecular planar structures of DSDTT (1) crystal structures corroborate strong intra/intermolecular $\pi-\pi$ orbital overlap favoring charge transport in the solid state.

Charge Transport Measurements and Thin-Film Microstructural Characterization. The charge transport properties of all DSDTT (1−3) and DRDTT (1R−3R) semiconductors were investigated by fabricating OFETs with a bottom-gate top-contact (BGTC) device architecture. The semiconducting small molecular crystalline films were solution-sheared onto (2-phenylethyl)trichlorosilane (PETS)-modified SiO_2/Si substrates from 4 to 5 mg mL^{-1} anisole or 1,2-dichlorobenzene (DCB) solutions using shearing rates of 5−15 $\mu m\ s^{-1}$ and deposition temperatures of 60−70 °C in ambient,[48−52] and subjected to post thermal-annealing at 80 °C in vacuum. Uniaxially grown micro-ribbons covering the entire substrates (thickness of ∼50 nm) can be observed from the polarized optical microscopy (POM) images of 1 and 1R films under optimized conditions (see Figure 5c,f). The overall micro-ribbon length extends up to the millimeter-level, with the width of 1 crystals being larger. Discrete aggregates and partially continuous elongated grains are observed for the TT- and T-capped compound films (Figure 5a,b and d,e), respectively. As the backbone end groups enlarge from T to DTT, the molecular planarity and conjugation length increase, which favor the formation of continuous crystals and thus enhance charge transport. Au electrodes (60 nm thick) were then deposited on the top of the semiconductor layer through vacuum evaporation to complete the OFET devices. The source and drain contacts of our OFET devices were deposited perpendicularly to the solution-shearing direction, so that charge transport occurs along the long-axes crystal growth direction to maximize charge transport. The optimized OFET performance parameters of 1−3 and 1R−3R, including the

https://dx.doi.org/10.1021/acs.chemmater.9b03967
Chem. Mater. 2020, 32, 1422−1429

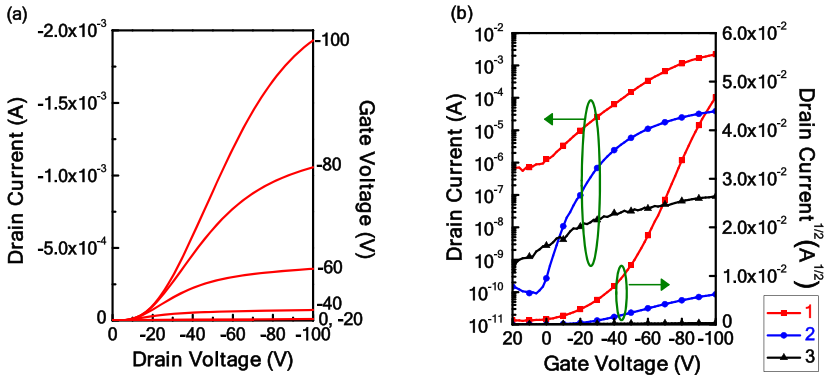

Figure 6. (a) Output characteristics of a 1-based OFET (at V_d = −100 V). (b) Transfer characteristics of DSDTT (1−3)-based OFETs.

maximum and average field effect mobilities (μ_{max} and μ_{avg}), ON/OFF current ratio (I_{ON}/I_{OFF}) and threshold voltage (V_{th}) are collected in Table 1 and representative transfer and output curves are shown in Figures 6, S9, and S10. The mobility distribution of the OFETs based on 1−3, 1R and 2R are reported in Figure S11. Note we followed suggested procedure for reporting OFET data acquisition and transport parameters.[53] All the devices behave as p-type FETs in both air and nitrogen. The mobility was evaluated from the slope of the plot of the drain current $(I_d)^{1/2}$ as a function of gate voltage (V_g) in the saturation region. Two trends in mobility are observed for our systems: (1) For both DSDTT and DRDTT families μ_{avg} increases dramatically when the π-conjugated unit, thus end-capped thiophene fused ring size, increases; (2) when comparing DSDTTs and DRDTTs with the same π-extension, μ_{avg} increases by more than ∼100×, thus increased structural planarity by intramolecular S···S non-covalent interactions greatly improves the charge transport, corroborating previous observations for intramolecularly locked molecular and polymeric semiconductors.[32] As a result, the μ_{max} of OFETs based on solution-sheared 1 micro-ribbon crystal remarkably reaches a value as high as 2.6 cm^2 V^{-1} s^{-1} with a V_{th} of −25.7 ± 15.8 V and I_{ON}/I_{OFF} of 10^4−10^5. Moreover, a relatively high μ_{avg} of 1.6 ± 0.5 cm^2 V^{-1} s^{-1} was obtained from 10 individual devices processed under similar conditions.

The molecular packing and microstructures in the solution-sheared organic semiconductor films were investigated by grazing incident X-ray diffraction (GIXRD) (Figures S12 and S13). The diffractograms of 3 are featureless and have no Bragg reflections (Figure S11c), indicating the absence of structural order in the film. This result agrees with the very weak field effect transistor behavior. In contrast, GIXRD of 1 and 2 (Figure S11b) exhibit pronounced out-of-plane (00l) scattering signals (c direction in the unit cell) thus corroborating the formation of ordered crystalline domains where the molecules adopt an edge-on orientation with respect to the substrate surface. The interlayer distance calculated from the primary peaks of 2 is 30.7 Å (at q_z of 0.20 Å^{-1}), which is almost twice the simulated width of the molecular backbone with an extended thiodecyl side chain, thus suggesting a bilayer periodicity resulting from partial intercalation of the side chains. The thiodecyl stacking distance for 1 is significantly shorter (23.9 Å) and several peaks assigned to higher order (00l) reflections are detected in the out-of-plane direction, demonstrating long-range ordering of interdigitated molecular stacking. Diffraction features associated with π−π stacking along the in-plane direction (h00) appear at q_{xy} = 1.33 Å^{-1} for 2 and 1.57 Å^{-1} for 1 corresponding to a π−π stacking distance of 4.7 and 4.0 Å, respectively. Furthermore, strong reflections for 1 are positioned along the direction of q_z at a given value of q_{xy}. This result indicates that 1 exhibits the strongest π−π intermolecular interactions, which is also in agreement with both the large red-shifted film optical absorption (Figure 2a) and large OFET mobility. In contrast, GIXRD data of the DRDTT films indicated that they are completely amorphous (1R) or reveal considerably reduced texturing (2R and 3R) and mostly randomly oriented crystallites compared with the DSDTTs (1−3), which is observed from the ring-type diffraction features and less long-range ordered scattering appearing at the scattering vector for the q_z direction (Figure S13). Note, using the solution-shearing technique for thin-film deposition can enhance crystallinity and promote out-of-plane molecular orientation as compared to that achieved for drop-cast films, as exemplified for 1 in Figure S14 where the latter films exhibit an arc-shaped diffraction. Finally, AFM imaging was utilized to analyze the surface morphologies of the OFET-optimized DSDTT semiconducting films. Compound 3 exhibit a long fibrous morphology comprising smaller domains with distinct grain boundary (Figure 5g). This poor film morphology agrees with the limited carrier mobility of 3 despite the planar and not irrelevant π structure comprising of 16 π-electrons (like tetrathiophene, 4T). For semiconductor 2 (Figure 5h) and 1 (Figure 5i) films AFM reveals the presence of large plate like grains consisting of flat terraces closely packed, morphological features which favor charge transport. It can be concluded that both the utilization of the shearing process and the achievement of stronger molecular interactions is likely responsible for the enhanced OFET performance.[45,51,54−56] On the other hand, among the DRDTT films only that of 1R exhibit crystal features, in agreement with the GIXRD analysis and the decent carrier mobility of this semiconductor.

CONCLUSIONS

In summary, a new series of intramolecular-locked semiconductors comprising DSDTT end-capped with DTT, TT, and T were designed and synthesized for solution-processed OFETs. Intramolecular S···S interactions promote planar structures and a more extended π-conjugation, as accessed by single crystal analysis and other physical properties, and enable hole mobilities as high as 2.6 cm^2 V^{-1} s^{-1}, which is ∼100× higher than the alkylated systems. Thus, from a structural and solid-state packing characteristic perspective this strategy can be seen equivalent to S-anellation/fusion of

https://dx.doi.org/10.1021/acs.chemmater.9b03967
Chem. Mater. 2020, 32, 1422−1429

thiophenes to afford *n*-thioacenes, however, with the advantage to be more synthetically accessible, provide more soluble and π-extended structures, as well as far larger charge transport capabilities than those achieved to date by *n*-thioacenes.

EXPERIMENTAL SECTION

Materials and Synthesis. All reagents were used as received from suppliers (Aldrich, Arco, and TCI) were used without additional purification unless indicated. All solvents (toluene, ether, and tetrahydrofuran) were distilled under nitrogen from Na/BPK while halogenated solvents were distilled from CaH_2. Synthetic routes to compounds 1−3 and 1R−3R are reported in the Supporting Information.

Characterization. ^1H and ^{13}C NMR spectra were recorded using a Bruker 500 or 300 instruments. Elemental analyses were performed with a Heraeus CHN-O-Rapid instrument. Mass spectrometric data were obtained with a JMS-700 high-resolution mass spectrometry (HRMS) instrument. Differential scanning calorimetry (DSC) was carried out under N_2 on a Mettler DSC 822 instrument (scanning rate = 10 °C min^{-1}). Thermogravimetric analysis (TGA) was carried out using a PerkinElmer TGA-7 thermal analysis system using dry N_2 as the carrier gas (flow rate = 10 mL min^{-1}; heating rate = 10 °C min^{-1}) and decomposition temperatures are the temperature when 5% mass loss occurs. Differential pulse voltammetry measurements were carried out using a three-electrode platform (a Pt disk working electrode, an Pt auxiliary electrode, and a non-aqueous Ag reference electrode, using a 0.1 M $TBAPF_6$ supporting electrolyte in the specified dry solvent) using a CHI621C Electrochemical Analyzer (CH Instruments). All electrochemical potentials were referenced to Fc^+/Fc (at +0.6 V). Single crystal structure analyses were collected with a Bruker Kappa Apex II charge-coupled device (CCD) diffractometer. UV−vis absorption spectra were measured on a JASCO V-530 spectrometer. The thickness of solution-sheared organic semiconductor film was measured with a DEKTAK 150 Surface Profilometer (Veeco). Atomic force microscopy (AFM) data were obtained with a Seiko SPA400 in air. NANOSENSORS Si tips with spring constant of 42 N m^{-1} and resonant frequency of 330 kHz were used for tapping mode AFM measurements. Grazing incident X-ray diffraction (GIXRD) was collected at beamline TLS 13A1/17A1 at National Synchrotron Radiation Research Center (NSRRC) of Taiwan.

Device Fabrication and Measurement. Charge transport measurements were carried out on OFETs fabricated using a bottom-gate top-contact device architecture. A highly doped silicon wafer with 300 nm of thermally growth SiO_2 [capacitance (C) of 10 nF cm^{-2}] was used as the gate/dielectric/substrate platform, which was successively cleaned by sonication in deionized water and isopropanol for 5 min each, dried under nitrogen flow and then treated with oxygen plasma (5 min, 100 W). Dielectric surface passivation was performed by using (2-phenylethyl)trichlorosilane (PETS) from 1 mM solution in toluene at 55 °C for 60 min. Organic semiconductor films were deposited on PETS/SiO_2/Si substrates by solution-shearing. The organic semiconductor solution was 2−5 mg mL^{-1} in anisole or 1,2-dichlorobenzene (DCB) or chlorobenzene (CB). Solution-sheared films were deposited at a shearing rate of 5−60 μm s^{-1} and a holding deposition temperature of 40−80 °C. The substrate was transferred to a vacuum chamber at a pressure of $<10^{-6}$ Torr and 70 nm thick Au, serving as source/drain contacts, was deposited with a rate of 0.5 Å s^{-1} on the masked organic semiconductors layers. The mobility (μ) of OFET devices was extracted using the following equation(saturation region): $I_d = (W/2L)C\mu(V_g - V_{th})^2$, where W is the channel width (1000 μm), L is the channel length (25 μm), V_g is the gate voltage, V_{th} is the threshold voltage, and I_d is the drain current. Devices were measured under nitrogen in a glovebox. Mobility values calculated from a gate voltage range of −30 to −50 V at a drain voltage (V_d) of −100 V. The current−voltage (I−V) characteristics of OFETs were recorded in a nitrogen glove box or ambient atmosphere with a Keithley 4200-SCS semiconductor parameter analyzer.

ASSOCIATED CONTENT

Supporting Information

The Supporting Information is available free of charge at https://pubs.acs.org/doi/10.1021/acs.chemmater.9b03967.

Synthetic details of all compounds; DSC, TGA, UV thin films of all compounds; optical absorption of compounds 1 and 1R at variable temperature, DFT derived HOMO and LUMO's; Single crystal structures of 1 and 1R; POM images of solution-sheared thin film; output characteristics; transfer characteristics; GIXRD diffraction pattern images of solution-sheared thin film; AFM images of thin film (Figures S1−S14 and Tables S1−S3) (PDF)

AUTHOR INFORMATION

Corresponding Authors

Cheng-Liang Liu − *Department of Chemical and Materials Engineering and Research Center of New Generation Light Driven Photovoltaic Module, National Central University, Taoyuan 32001, Taiwan*; Email: clliu@ncu.edu.tw

Ming-Chou Chen − *Department of Chemistry and Research Center of New Generation Light Driven Photovoltaic Module, National Central University, Taoyuan 32001, Taiwan*; Email: mcchen@ncu.edu.tw

Antonio Facchetti − *Department of Chemistry, Northwestern University, Evanston, Illinois 60208, United States*; Email: a-facchetti@northwestern.edu

Authors

Sureshraju Vegiraju − *Department of Chemistry and Research Center of New Generation Light Driven Photovoltaic Module, National Central University, Taoyuan 32001, Taiwan*

Xian-Lun Luo − *Department of Chemical and Materials Engineering and Research Center of New Generation Light Driven Photovoltaic Module, National Central University, Taoyuan 32001, Taiwan*

Long-Huan Li − *Department of Chemistry and Research Center of New Generation Light Driven Photovoltaic Module, National Central University, Taoyuan 32001, Taiwan*

Shakil N. Afraj − *Department of Chemistry and Research Center of New Generation Light Driven Photovoltaic Module, National Central University, Taoyuan 32001, Taiwan*

Chi Lee − *Department of Chemistry and Research Center of New Generation Light Driven Photovoltaic Module, National Central University, Taoyuan 32001, Taiwan*

Ding Zheng − *Department of Chemistry, Northwestern University, Evanston, Illinois 60208, United States*

Hsin-Chun Hsieh − *Department of Chemistry and Research Center of New Generation Light Driven Photovoltaic Module, National Central University, Taoyuan 32001, Taiwan*

Chia-Chi Lin − *Department of Chemical and Materials Engineering and Research Center of New Generation Light Driven Photovoltaic Module, National Central University, Taoyuan 32001, Taiwan*

Shao-Huan Hong − *Department of Chemical and Materials Engineering and Research Center of New Generation Light Driven Photovoltaic Module, National Central University, Taoyuan 32001, Taiwan*

Hsin-Chia Tsai − *Department of Chemistry and Research Center of New Generation Light Driven Photovoltaic Module, National Central University, Taoyuan 32001, Taiwan*

https://dx.doi.org/10.1021/acs.chemmater.9b03967
Chem. Mater. 2020, 32, 1422−1429

Gene-Hsiang Lee − *Instrumentation Center, National Taiwan University, Taipei 10617, Taiwan*
Shih-Huang Tung − *Institute of Polymer Science and Engineering, National Taiwan University, Taipei 10617, Taiwan*

Complete contact information is available at: https://pubs.acs.org/10.1021/acs.chemmater.9b03967

Author Contributions

[#]S.V. and X.-L.L. contributed equally to this work.

Notes

The authors declare no competing financial interest.

■ ACKNOWLEDGMENTS

The authors gratefully acknowledge the funding from the Ministry of Science and Technology (MOST) of Taiwan. The authors thank Beamline TLS 13A1/17A1/23A1 [National Synchrotron Radiation Research Center (NSRRC) of Taiwan] for providing beamtime.

■ REFERENCES

(1) Fukuda, K.; Takeda, Y.; Yoshimura, Y.; Shiwaku, R.; Tran, L. T.; Sekine, T.; Mizukami, M.; Kumaki, D.; Tokito, S. Fully-printed high-performance organic thin-film transistors and circuitry on one-micron-thick polymer films. *Nat. Commun.* **2014**, *5*, 4147.
(2) Guo, X. G.; Facchetti, A.; Marks, T. J. Imide- and Amide-Functionalized Polymer Semiconductors. *Chem. Rev.* **2014**, *114*, 8943.
(3) Osaka, I.; Takimiya, K. Naphthobischalcogenadiazole Conjugated Polymers: Emerging Materials for Organic Electronics. *Adv. Mater.* **2017**, *29*, 1605218.
(4) Xiao, K.; Liu, Y.; Qi, T.; Zhang, W.; Wang, F.; Gao, J.; Qiu, W.; Ma, Y.; Cui, G.; Chen, S.; Zhan, X.; Yu, G.; Qin, J.; Hu, W.; Zhu, D. A Highly π-Stacked Organic Semiconductor for Field-Effect Transistors Based on Linearly Condensed Pentathienoacene. *J. Am. Chem. Soc.* **2005**, *127*, 13281.
(5) Chakravarthi, N.; Gunasekar, K.; Cho, W.; Long, D. X.; Kim, Y.-H.; Song, C. E.; Lee, J.-C.; Facchetti, A.; Song, M.; Noh, Y.-Y.; Jin, S.-H. A simple structured and efficient triazine-based molecule as an interfacial layer for high performance organic electronics. *Energy Environ. Sci.* **2016**, *9*, 2595.
(6) Fei, Z.; Chen, L.; Han, Y.; Gann, E.; Chesman, A. S. R.; McNeill, C. R.; Anthopoulos, T. D.; Heeney, M.; Pietrangelo, A. Alternating 5,5-Dimethylcyclopentadiene and Diketopyrrolopyrrole Copolymer Prepared at Room Temperature for High Performance Organic Thin-Film Transistors. *J. Am. Chem. Soc.* **2017**, *139*, 8094.
(7) Wang, C.; Dong, H.; Hu, W.; Liu, Y.; Zhu, D. Semiconducting π-Conjugated Systems in Field-Effect Transistors: A Material Odyssey of Organic Electronics. *Chem. Rev.* **2012**, *112*, 2208.
(8) Takimiya, K.; Shinamura, S.; Osaka, I.; Miyazaki, E. Thienoacene-Based Organic Semiconductors. *Adv. Mater.* **2011**, *23*, 4347.
(9) Takimiya, K.; Osaka, I.; Mori, T.; Nakano, M. Organic Semiconductors Based on [1]Benzothieno[3,2-b][1]benzothiophene Substructure. *Acc. Chem. Res.* **2014**, *47*, 1493.
(10) Xue, G. B.; Fan, C. C.; Wu, J. K.; Liu, S.; Liu, Y. J.; Chen, H. Z.; Xin, H. L.; Li, H. Y. Ambipolar charge transport of TIPS-pentacene single-crystals grown from non-polar solvents. *Mater. Horiz.* **2015**, *2*, 344.
(11) James, D. I.; Wang, S.; Ma, W.; Hedström, S.; Meng, X.; Persson, P.; Fabiano, S.; Crispin, X.; Andersson, M. R.; Berggren, M.; Wang, E. High-Performance Hole Transport and Quasi-Balanced Ambipolar OFETs Based on D−A−A Thieno-benzo-isoindigo Polymers. *Adv. Electron. Mater.* **2016**, *2*, 1500313.
(12) Wang, S.; Sun, H.; Ail, U.; Vagin, M.; Persson, P. O. Å.; Andreasen, J. W.; Thiel, W.; Berggren, M.; Crispin, X.; Fazzi, D.; Fabiano, S. Thermoelectric Properties of Solution-Processed n-Doped Ladder-Type Conducting Polymers. *Adv. Mater.* **2016**, *28*, 10764.
(13) Fan, C.; Zoombelt, A. P.; Jiang, H.; Fu, W.; Wu, J.; Yuan, W.; Wang, Y.; Li, H.; Chen, H.; Bao, Z. Solution-Grown Organic Single-Crystalline p-n Junctions with Ambipolar Charge Transport. *Adv. Mater.* **2013**, *25*, 5762.
(14) Do, T.-T.; Takeda, Y.; Manzhos, S.; Bell, J.; Tokito, S.; Sonar, P. Naphthalimide end capped anthraquinone based solution-processable n-channel organic semiconductors: effect of alkyl chain engineering on charge transport. *J. Mater. Chem. C* **2018**, *6*, 3774.
(15) Cheng, S. S.; Huang, P. Y.; Ramesh, M.; Chang, H. C.; Chen, L. M.; Yeh, C. M.; Fung, C. L.; Wu, M. C.; Liu, C. C.; Kim, C.; Lin, H. C.; Chen, M. C.; Chu, C. W. Solution-Processed Small-Molecule Bulk Heterojunction Ambipolar Transistors. *Adv. Funct. Mater.* **2014**, *24*, 2057.
(16) Dou, J.-H.; Zheng, Y.-Q.; Yao, Z.-F.; Yu, Z.-A.; Lei, T.; Shen, X.; Luo, X.-Y.; Sun, J.; Zhang, S.-D.; Ding, Y.-F.; Han, G.; Yi, Y.; Wang, J.-Y.; Pei, J. Fine-Tuning of Crystal Packing and Charge Transport Properties of BDOPV Derivatives through Fluorine Substitution. *J. Am. Chem. Soc.* **2015**, *137*, 15947.
(17) Yuan, Y. B.; Giri, G.; Ayzner, A. L.; Zoombelt, A. P.; Mannsfeld, S. C. B.; Chen, J. H.; Nordlund, D.; Toney, M. F.; Huang, J. S.; Bao, Z. N. Ultra-high mobility transparent organic thin film transistors grown by an off-centre spin-coating method. *Nat. Commun.* **2014**, *5*, 3005.
(18) Chen, H.-Y.; Schweicher, G.; Planells, M.; Ryno, S. M.; Broch, K.; White, A. J. P.; Simatos, D.; Little, M.; Jellett, C.; Cryer, S. J.; Marks, A.; Hurhangee, M.; Brédas, J.-L.; Sirringhaus, H.; McCulloch, I. Crystal Engineering of Dibenzothiophenothieno[3,2-b]thiophene (DBTTT) Isomers for Organic Field-Effect Transistors. *Chem. Mater.* **2018**, *30*, 7587.
(19) Mei, J. G.; Diao, Y.; Appleton, A. L.; Fang, L.; Bao, Z. N. Integrated Materials Design of Organic Semiconductors for Field-Effect Transistors. *J. Am. Chem. Soc.* **2013**, *135*, 6724.
(20) Wu, J. K.; Li, Q. F.; Xue, G. B. A.; Chen, H. Z.; Li, H. Y. Preparation of Single-Crystalline Heterojunctions for Organic Electronics. *Adv. Mater.* **2017**, *29*, 1606101.
(21) Fan, C. C.; Zoombelt, A. P.; Jiang, H.; Fu, W. F.; Wu, J. K.; Yuan, W. T.; Wang, Y.; Li, H. Y.; Chen, H. Z.; Bao, Z. N. Solution-Grown Organic Single-Crystalline p-n Junctions with Ambipolar Charge Transport. *Adv. Mater.* **2013**, *25*, 5762.
(22) Jiang, W.; Li, Y.; Wang, Z. Heteroarenes as high performance organic semiconductors. *Chem. Soc. Rev.* **2013**, *42*, 6113.
(23) Jiang, W.; Li, Y.; Wang, Z. H. Heteroarenes as high performance organic semiconductors. *Chem. Soc. Rev.* **2013**, *42*, 6113.
(24) Shi, S.; Wang, H.; Uddin, M. A.; Yang, K.; Su, M.; Bianchi, L.; Chen, P.; Cheng, X.; Guo, H.; Zhang, S.; Woo, H. Y.; Guo, X. Head-to-Head Linked Dialkylbifuran-Based Polymer Semiconductors for High-Performance Organic Thin-Film Transistors with Tunable Charge Carrier Polarity. *Chem. Mater.* **2019**, *31*, 1808.
(25) Di Maria, F.; Olivelli, P.; Gazzano, M.; Zanelli, A.; Biasiucci, M.; Gigli, G.; Gentili, D.; D'Angelo, P.; Cavallini, M.; Barbarella, G. A Successful Chemical Strategy To Induce Oligothiophene Self-Assembly into Fibers with Tunable Shape and Function. *J. Am. Chem. Soc.* **2011**, *133*, 8654.
(26) Salatelli, E.; Marinelli, M.; Lanzi, M.; Zanelli, A.; Dell'Elce, S.; Liscio, A.; Gazzano, M.; Di Maria, F. Bulk Heterojunction Solar Cells: The Role of Alkyl Side Chain on Nanoscale Morphology of Sulfur Over-rich Regioregular Polythiophene/Fullerene Blends. *J. Phys. Chem. C* **2018**, *122*, 4156.
(27) Vegiraju, S.; Chang, B.-C.; Priyanka, P.; Huang, D.-Y.; Wu, K.-Y.; Li, L.-H.; Chang, W.-C.; Lai, Y.-Y.; Hong, S.-H.; Yu, B.-C.; Wang, C.-L.; Chang, W.-J.; Liu, C.-L.; Chen, M.-C.; Facchetti, A. Intramolecular Locked Dithioalkylbithiophene-Based Semiconductors for High-Performance Organic Field-Effect Transistors. *Adv. Mater.* **2017**, *29*, 1702414.
(28) Shaw, C. M.; Zhang, X.; San Miguel, L.; Matzger, A. J.; Martin, D. C. Synthesis and structure of α-substituted pentathienoacenes. *J. Mater. Chem. C* **2013**, *1*, 3686.

(29) Xiao, K.; Liu, Y.; Qi, T.; Zhang, W.; Wang, F.; Gao, J.; Qiu, W.; Ma, Y.; Cui, G.; Chen, S.; Zhan, X.; Yu, G.; Qin, J.; Hu, W.; Zhu, D. A Highly π-Stacked Organic Semiconductor for Field-Effect Transistors Based on Linearly Condensed Pentathienoacene. *J. Am. Chem. Soc.* **2005**, *127*, 13281.
(30) Liu, Y.; Sun, X.; Di, C.-a.; Liu, Y.; Du, C.; Lu, K.; Ye, S.; Yu, G. Hexathienoacene: Synthesis, Characterization, and Thin-Film Transistors. *Chem. Asian J.* **2010**, *5*, 1550.
(31) Huang, H.; Chen, Z.; Ortiz, R. P.; Newman, C.; Usta, H.; Lou, S.; Youn, J.; Noh, Y.-Y.; Baeg, K.-J.; Chen, L. X.; Facchetti, A.; Marks, T. Combining Electron-Neutral Building Blocks with Intramolecular "Conformational Locks" Affords Stable, High-Mobility P- and N-Channel Polymer Semiconductors. *J. Am. Chem. Soc.* **2012**, *134*, 10966.
(32) Huang, H.; Yang, L.; Facchetti, A.; Marks, T. J. Organic and Polymeric Semiconductors Enhanced by Noncovalent Conformational Locks. *Chem. Rev.* **2017**, *117*, 10291.
(33) Kawashima, K.; Fukuhara, T.; Suda, Y.; Suzuki, Y.; Koganezawa, T.; Yoshida, H.; Ohkita, H.; Osaka, I.; Takimiya, K. Implication of Fluorine Atom on Electronic Properties, Ordering Structures, and Photovoltaic Performance in Naphthobisthiadiazole-Based Semiconducting Polymers. *J. Am. Chem. Soc.* **2016**, *138*, 10265.
(34) Guo, X.; Liao, Q.; Manley, E. F.; Wu, Z.; Wang, Y.; Wang, W.; Yang, T.; Shin, Y.-E.; Cheng, X.; Liang, Y.; Chen, L. X.; Baeg, K.-J.; Marks, T. J.; Guo, X. Materials Design via Optimized Intramolecular Noncovalent Interactions for High-Performance Organic Semiconductors. *Chem. Mater.* **2016**, *28*, 2449.
(35) Yu, S.; Peng, A.; Zhang, S.; Huang, H. Noncovalent conformational locks in organic semiconductors. *Sci. China Chem.* **2018**, *61*, 1359.
(36) Zhang, W.; Mao, Z.; Zheng, N.; Zou, J.; Wang, L.; Wei, C.; Huang, J.; Gao, D.; Yu, G. Highly planar cross-conjugated alternating polymers with multiple conformational locks: synthesis, characterization and their field-effect properties. *J. Mater. Chem. C* **2016**, *4*, 9266.
(37) Zheng, Y.-Q.; Lei, T.; Dou, J.-H.; Xia, X.; Wang, J.-Y.; Liu, C.-J.; Pei, J. Strong Electron-Deficient Polymers Lead to High Electron Mobility in Air and Their Morphology-Dependent Transport Behaviors. *Adv. Mater.* **2016**, *28*, 7213.
(38) Dong, T.; Lv, L.; Feng, L.; Xia, Y.; Deng, W.; Ye, P.; Yang, B.; Ding, S.; Facchetti, A.; Dong, H.; Huang, H. Noncovalent Se···O Conformational Locks for Constructing High-Performing Optoelectronic Conjugated Polymers. *Adv. Mater.* **2017**, *29*, 1606025.
(39) Vegiraju, S.; Chang, B. C.; Priyanka, P.; Huang, D. Y.; Wu, K. Y.; Li, L. H.; Chang, W. C.; Lai, Y. Y.; Hong, S. H.; Yu, B. C.; Wang, C. L.; Chang, W. J.; Liu, C. L.; Chen, M. C.; Facchetti, A. Intramolecular Locked Dithioalkylbithiophene-Based Semiconductors for High-Performance Organic Field-Effect Transistors. *Adv. Mater.* **2017**, *29*, 1702414.
(40) Li, Y.; Wu, Y.; Liu, P.; Birau, M.; Pan, H.; Ong, B. S. Poly(2,5-bis(2-thienyl)-3,6-dialkylthieno [3,2-b]thiophene)s—High-Mobility Semiconductors for Thin-Film Transistors. *Adv. Mater.* **2006**, *18*, 3029.
(41) Sun, Y. M.; Ma, Y. Q.; Liu, Y. Q.; Lin, Y. Y.; Wang, Z. Y.; Wang, Y.; Di, C. A.; Xiao, K.; Chen, X. M.; Qiu, W. F.; Zhang, B.; Yu, G.; Hu, W. P.; Zhu, D. B. High-Performance and Stable Organic Thin-Film Transistors Based on Fused Thiophenes. *Adv. Funct. Mater.* **2006**, *16*, 426.
(42) Zhang, L.; Tan, L.; Wang, Z.; Hu, W.; Zhu, D. High-Performance, Stable Organic Field-Effect Transistors Based on trans-1,2-(Dithieno[2,3-b:3′,2′-d]thiophene)ethene. *Chem. Mater.* **2009**, *21*, 1993.
(43) Youn, J.; Huang, P.-Y.; Huang, Y.-W.; Chen, M.-C.; Lin, Y.-J.; Huang, H.; Ortiz, R. P.; Stern, C.; Chung, M.-C.; Feng, C.-Y.; Chen, L.-H.; Facchetti, A.; Marks, T. J. Versatile α,ω-Disubstituted Tetrathienoacene Semiconductors for High Performance Organic Thin-Film Transistors. *Adv. Funct. Mater.* **2012**, *22*, 48.
(44) Chen, M.-C.; Vegiraju, S.; Huang, C.-M.; Huang, P.-Y.; Prabakaran, K.; Yau, S. L.; Chen, W.-C.; Peng, W.-T.; Chao, I.; Kim, C.; Tao, Y.-T. Asymmetric fused thiophenes for field-effect transistors: crystal structure-film microstructure-transistor performance correlations. *J. Mater. Chem. C* **2014**, *2*, 8892.
(45) Vegiraju, S.; He, G.-Y.; Kim, C.; Priyanka, P.; Chiu, Y.-J.; Liu, C.-W.; Huang, C.-Y.; Ni, J.-S.; Wu, Y.-W.; Chen, Z.; Lee, G.-H.; Tung, S.-H.; Liu, C.-L.; Chen, M.-C.; Facchetti, A. Solution-Processable Dithienothiophenoquinoid (DTTQ) Structures for Ambient-Stable n-Channel Organic Field Effect Transistors. *Adv. Funct. Mater.* **2017**, *27*, 1606761.
(46) Chen, M.-C.; Chiang, Y.-J.; Kim, C.; Guo, Y.-J.; Chen, S.-Y.; Liang, Y.-J.; Huang, Y.-W.; Hu, T.-S.; Lee, G.-H.; Facchetti, A.; Marks, T. J. One-pot [1 + 1 + 1] synthesis of dithieno[2,3-b:3[prime or minute],2[prime or minute]-d]thiophene (DTT) and their functionalized derivatives for organic thin-film transistors. *Chem. Commun.* **2009**, 1846.
(47) Xue, Z.; Chen, S.; Gao, N.; Xue, Y.; Lu, B.; Watson, O. A.; Zang, L.; Xu, J. Structural Design and Applications of Stereoregular Fused Thiophenes and Their Oligomers and Polymers. *Polym. Rev.* **2019**, 1−41.
(48) Diao, Y.; Shaw, L.; Bao, Z.; Mannsfeld, S. C. B. Morphology control strategies for solution-processed organic semiconductor thin films. *Energy Environ. Sci.* **2014**, *7*, 2145.
(49) Giri, G.; DeLongchamp, D. M.; Reinspach, J.; Fischer, D. A.; Richter, L. J.; Xu, J.; Benight, S.; Ayzner, A.; He, M.; Fang, L.; Xue, G.; Toney, M. F.; Bao, Z. Effect of Solution Shearing Method on Packing and Disorder of Organic Semiconductor Polymers. *Chem. Mater.* **2015**, *27*, 2350.
(50) Shaw, L.; Hayoz, P.; Diao, Y.; Reinspach, J. A.; To, J. W. F.; Toney, M. F.; Weitz, R. T.; Bao, Z. Direct Uniaxial Alignment of a Donor−Acceptor Semiconducting Polymer Using Single-Step Solution Shearing. *ACS Appl. Mater. Interfaces* **2016**, *8*, 9285.
(51) Diao, Y.; Tee, B. C. K.; Giri, G.; Xu, J.; Kim, D. H.; Becerril, H. A.; Stoltenberg, R. M.; Lee, T. H.; Xue, G.; Mannsfeld, S. C. B.; Bao, Z. Solution coating of large-area organic semiconductor thin films with aligned single-crystalline domains. *Nat. Mater.* **2013**, *12*, 665.
(52) Gu, X.; Shaw, L.; Gu, K.; Toney, M. F.; Bao, Z. The meniscus-guided deposition of semiconducting polymers. *Nat. Commun.* **2018**, *9*, 534.
(53) Choi, D.; Chu, P.-H.; McBride, M.; Reichmanis, E. Best Practices for Reporting Organic Field Effect Transistor Device Performance. *Chem. Mater.* **2015**, *27*, 4167.
(54) Giri, G.; Verploegen, E.; Mannsfeld, S. C. B.; Atahan-Evrenk, S.; Kim, D. H.; Lee, S. Y.; Becerril, H. A.; Aspuru-Guzik, A.; Toney, M. F.; Bao, Z. Tuning charge transport in solution-sheared organic semiconductors using lattice strain. *Nature* **2011**, *480*, 504.
(55) Jo, G.; Jeong, J. W.; Choi, S.; Kim, H.; Park, J. J.; Jung, J.; Chang, M. Large-Scale Alignment of Polymer Semiconductor Nanowires for Efficient Charge Transport via Controlled Evaporation of Confined Fluids. *ACS Appl. Mater. Interfaces* **2019**, *11*, 1135.
(56) Bulgarevich, K.; Sakamoto, K.; Minari, T.; Yasuda, T.; Miki, K. Spatially Uniform Thin-Film Formation of Polymeric Organic Semiconductors on Lyophobic Gate Insulator Surfaces by Self-Assisted Flow-Coating. *ACS Appl. Mater. Interfaces* **2017**, *9*, 6237.

https://dx.doi.org/10.1021/acs.chemmater.9b03967
Chem. Mater. 2020, 32, 1422−1429